



Theoretical-experimental evaluation of the photocatalytic activity of $\text{KCa}_2\text{Ta}_{3-x}\text{Nb}_x\text{O}_{10}$



Arnayra S. Brito^a, Valerie Bouquet^b, Valerie Demange^b, François Cheviré^b, Maryline Guilloux-Viry^b, Thiago D. Marinho^a, Juliana K.D. Souza^a, Lais C. Lima^a, Nayara A. Pinheiro^a, Ieda M.G. Santos^a, Julio R. Sambrano^c, Anderson R. Albuquerque^d, Ary S. Maia^{a,*}

^a NPE-LACOM – Federal University of Paraíba, 58051-900 João Pessoa, PB, Brazil

^b Univ. Rennes, CNRS, ISCR – UMR 6226, ScanMat – UMS 2001, F-35000 Rennes, France

^c Modeling and Molecular Simulation Group, INCTMN-UNESP, São Paulo State University, Bauru, SP, Brazil

^d Chemistry Institute, Federal University of Rio Grande do Norte, 59078-970 Natal, RN, Brazil

ARTICLE INFO

Article history:

Received 17 May 2019

Received in revised form 21 June 2019

Accepted 1 July 2019

Available online 2 July 2019

Keywords:

DFT

Dion-Jacobson perovskite

Tantaloniobates

Octahedra distortion

ABSTRACT

$\text{KCa}_2\text{Ta}_{3-x}\text{Nb}_x\text{O}_{10}$ samples were synthesized by solid-state reaction and evaluated on the hydroxylation of terephthalic acid under UVC irradiation. Computational simulations via DFT were carried out in order to study their structural and electronic properties. Theoretical results show good agreement with experimental data, regarding lattice parameters and band-gap energy values and indicated that the photocatalytic performance for hydroxyl radicals production is directly related to the degree of octahedral distortions in these materials.

© 2019 Elsevier B.V. All rights reserved.

1. Introduction

Dion-Jacobson-type (D-J) perovskites have drawn attention for their physical and chemical properties, particularly for their photocatalytic activity [1–4]. They have molecular formula $A_x[B_{m-1}M_nO_{3m+1}]$ (where A is an alkaline ion; B an alkaline earth ion; M a transition metal and n indicates the number of $[\text{MO}_6]$ octahedra that form each perovskite-like slab) [5]. Some authors relate the photocatalytic activity of perovskites to the degree of octahedron distortion [6–8]. The main objective of this work was to study tantaloniobates ($\text{KCa}_2\text{Ta}_{3-x}\text{Nb}_x\text{O}_{10}$, $x = 0, 1$ and 2) with D-J perovskite structure and to evaluate the effect of Ta:Nb ratio on their structural and photocatalytic properties.

2. Experimental

Materials were synthesized by solid-state reaction using carbonates or oxides as precursors under temperatures between 1100 and 1200 °C. Synthesized materials were characterized by X-ray diffraction (XRD, Bruker D8 Advance, $\text{CuK}\alpha 1$), Diffuse Reflectance Spectroscopy (DRS, Varian Cary 100 UV–Vis, 250–800 nm),

* Corresponding author.

E-mail address: arymaia@quimica.ufpb.br (A.S. Maia).

Raman spectroscopy (Renishaw inVia Raman Microscope, 514 nm laser wavelength), SEM-EDXS (Jeol JSM 7100F microscope, operating at 10 kV for Energy Dispersive X-ray Spectroscopy analyses (EDXS) using an Oxford Instruments AZtec system). Formation of hydroxyl radicals was evaluated by the photohydroxylation of terephthalic acid (TA), used as probe at room temperature [9], under conditions previously described in the literature [10]. A blank test was performed with TA solution irradiation without photocatalyst. Formation of the luminescent 2-hydroxyterephthalic acid (HTA) was evaluated by spectrofluorimetry (Shimadzu RF-5301PC). Further details of syntheses and characterizations are displayed in the [Supplementary Data \(SD-01\)](#).

3. Computational details

Periodic DFT calculations were performed with CRYSTAL17 software [11] by using the global hybrid functional PBE0. $\text{KCa}_2\text{Ta}_3\text{O}_{10}$ and $\text{KCa}_2\text{Nb}_3\text{O}_{10}$ are layered perovskites with orthorhombic structures ($C222$ and $Cmcm$ space groups respectively) and a slab constituted by the stacking of three corner-connected octahedra $[\text{Nb}/\text{TaO}_6]$. In the absence of information about $\text{KCa}_2\text{TaNb}_2\text{O}_{10}$ and $\text{KCa}_2\text{Ta}_2\text{NbO}_{10}$ symmetry space group and for purpose of comparison, all materials were calculated in the $\text{KCa}_2\text{Ta}_3\text{O}_{10}$ ($C222$)

space group. There are two distinct crystallographic positions for the transition metals, two equivalent octahedra (Oct1) constituting the slab edges while the other one (Oct2) forms the inner layer. For purposes of computational models depending on the chemical composition Nb and/or Ta were ascribed to either crystallographic positions without considering any mixed occupations. Band structure and density of states (DOS) calculations were plotted employing the same k -points set as the diagonalization of the Fock matrix for optimization process. Distortion index was based on bond lengths as proposed by Baur [12] and the effective coordination number was calculated as the sum of the so-called “bond weight” of all polyhedron bonds. Further details of computational simulations are displayed in [Supplementary Data \(SD-02\)](#).

4. Results and discussion

XRD patterns ([Fig. 1\(1\)](#)) confirmed the formation of the targeted phases with small amount of KNbO_3 . Progressive substitution of tantalum by niobium atoms in the structure did not significantly modify the observed reflections except for small displacements of the peaks. $\text{KCa}_2\text{Ta}_3\text{O}_{10}$ pattern was indexed by ICDD 01-089-8542, in agreement to literature [2]. No significant morphological changes were observed for the synthesized materials, as evidenced by SEM results (SD-03) and large surfaces assigned to (0 1 0) planes were observed [13]. Stoichiometry of the samples was confirmed by SEM-EDXS ([Table 1](#)).

Raman spectra ([Fig. 1\(2\)](#)) evidenced the existence of two different types of octahedra, a highly distorted one (Oct1), which occupies the slab edge (bands around 930 and 600 cm^{-1}) and a slightly distorted one (Oct2) that occupies the lamella center (bands around 770 cm^{-1}). These patterns are in good agreement with the literature [14]. The substitution of Ta by Nb caused a

displacement of the bands around 770 and 600 cm^{-1} to smaller wavenumbers.

Band-gap energies of the synthesized materials were calculated using the Kubelka-Munk formalism [15] from DRS results (SD-04) and confirmed the downward trend as Ta is replaced by Nb ([Table 1](#)).

Photogeneration of hydroxyl radicals was evaluated by HTA formation, as function of reaction time ([Fig. 2\(1\)](#) and (2)). All of the materials had some activity when compared to the blank test, while $\text{KCa}_2\text{TaNb}_2\text{O}_{10}$ sample presented a much higher yield. The secondary phase (KNbO_3) showed no activity for this reaction. Literature results [3] indicate that no $\cdot\text{OH}$ radicals were generated for 2D-2D $g\text{-C}_3\text{N}_4/\text{KCa}_2\text{Nb}_3\text{O}_{10}$ nanosheet heterojunctions.

In an attempt to better understand the photocatalytic results, computational simulations were carried out focusing on structural and electronic aspects of the $\text{KCa}_2\text{Ta}_{3-x}\text{Nb}_x\text{O}_{10}$ phases. Similar data were not found in the literature for these systems. [Table 1](#) depicts the calculated cell parameters and the resulting deviations which were very low. Band structure (Figure SD-05) showed that all materials have indirect band-gap (X- Γ) and quite similar values were observed when comparing experimentally and theoretically calculated band-gap values ([Table 1](#)). These results, associated with XRD patterns for all samples, suggested that the previously assumed space group was valid.

The calculated atomic positions were used to construct the structures shown in [Fig. 3](#). Regardless the atom that occupied the octahedral site of the layer edge (Oct1), this octahedron presented greater distortion than the one in the inner layer (Oct2). However, when Nb occupied this site, with Ta in the central position ($\text{KCa}_2\text{TaNb}_2\text{O}_{10}$), the highest distortion index of these octahedra took place ([Fig. 3](#)). This distortion was so pronounced that this Nb tended to 5-fold coordination, due to the high value of the axial Nb-O bond length, directed to the $[\text{TaO}_6]$ octahedron. A tendency

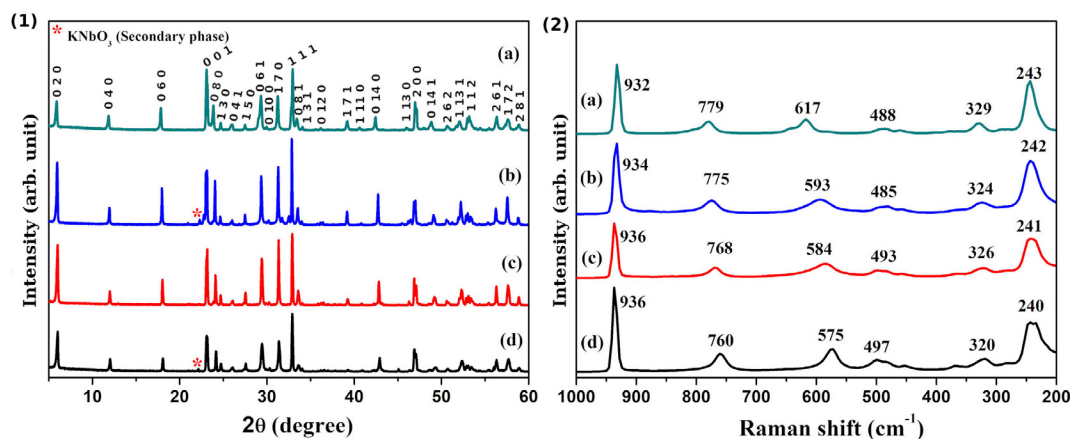


Fig. 1. XRD patterns (1) and Raman spectra (2) of $\text{KCa}_2\text{Ta}_3\text{O}_{10}$ (a), $\text{KCa}_2\text{Ta}_2\text{NbO}_{10}$ (b), $\text{KCa}_2\text{TaNb}_2\text{O}_{10}$ (c), $\text{KCa}_2\text{Nb}_3\text{O}_{10}$ (d).

Table 1

Experimental composition and band-gap energy (E_g) of the synthesized materials compared to theoretical results.

Samples	Experimental Results		Theoretical Results			
	Composition	E_g (eV)	a (Å)	b (Å)	c (Å)	E_g (eV)
$\text{KCa}_2\text{Ta}_3\text{O}_{10}$	$\text{K}_{0.8}\text{Ca}_2\text{Ta}_{2.9}\text{O}_{10}$	4.2	$3.9272 (+1.59\%)^*$	$28.533 (-4.18\%)^*$	$3.8856 (+0.87\%)^*$	4.29
$\text{KCa}_2\text{Ta}_2\text{NbO}_{10}$	$\text{K}_{1.1}\text{Ca}_2\text{Ta}_{2.1}\text{Nb}_{0.8}\text{O}_{10}$	3.8	3.9708	28.539	3.8810	3.68
$\text{KCa}_2\text{TaNb}_2\text{O}_{10}$	$\text{K}_{1.2}\text{Ca}_2\text{TaNb}_{1.9}\text{O}_{10}$	3.6	3.9530	28.552	3.9161	3.46
$\text{KCa}_2\text{Nb}_3\text{O}_{10}$	$\text{K}_{1.2}\text{Ca}_2\text{Nb}_{2.8}\text{O}_{10}$	3.5	3.9824	28.480	3.9169	3.41

* Percent deviations from the lattice parameters of ICDD 01-089-8542.

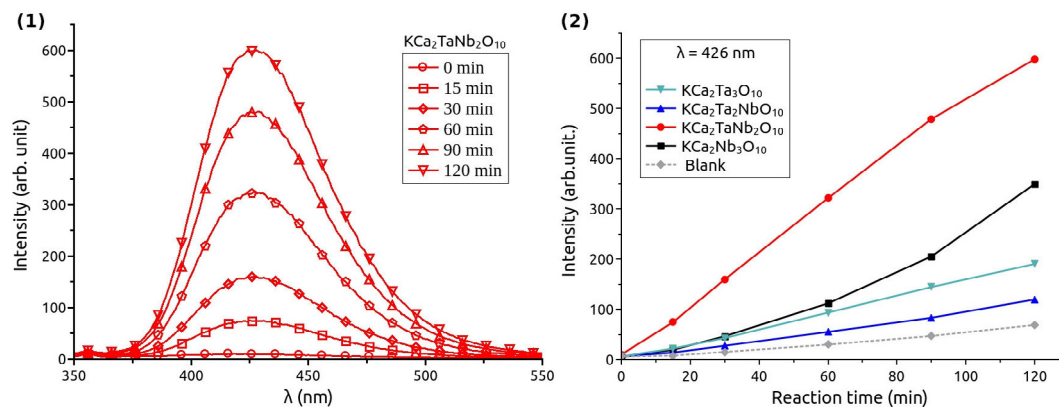


Fig. 2. Fluorescence spectra of HTA formed in the reaction catalyzed by $\text{KCa}_2\text{TaNb}_2\text{O}_{10}$ (1). Maximum intensity of HTA fluorescence produced by photohydroxylation of TA as a function of reaction time (2).

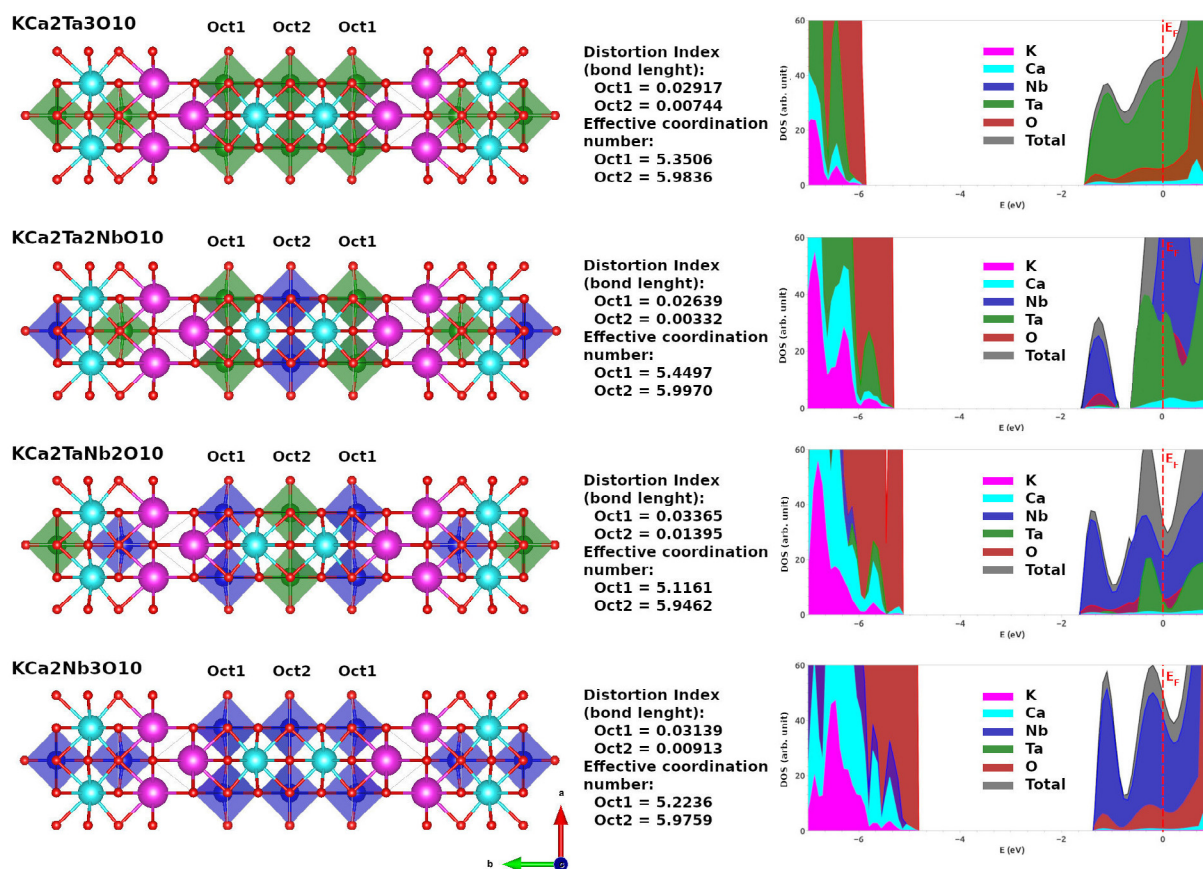


Fig. 3. Structural representation of the $\text{KCa}_2\text{Ta}_{3-x}\text{Nb}_x\text{O}_{10}$ phases, with octahedron distortion index, Nb/Ta effective coordination number and DOS results.

to increase tilting between octahedra along a axis, culminating with a decrease of approximately 18° in the Nb-O-Nb bond, can also be observed for $\text{KCa}_2\text{TaNb}_2\text{O}_{10}$ (Figure SD-06).

A marked shift of the Fermi level towards the conduction band (CB) was also observed in the band structure (Figure SD-04), similar to Burstein-Moss shift [16], which indicates the need to expand the electronic evaluation of theoretical calculations.

According to DOS (Figure SD-05) the valence band (VB) was mainly constituted by oxygen atoms, whereas the conduction band had greater participation of metal atoms. A detail of VB and CB edges is presented in Fig. 3.

Due to its higher electronegativity, as usually assigned [8] 4d states of Nb lies lower than 5d state of Ta and thus participates preponderantly to the CB edge for all Nb-containing structures, regardless of its proportion or its location. A deepening of theoretical calculations regarding electronic effects is already underway and will be released soon in the form of a new theoretical article.

Correlating the experimental data of hydroxyl radicals photo-generation with theoretical calculations results, it is evident that the increasing order of photocatalytic activity is exactly the same for the octahedron distortion index in this triple-layered D-J perovskite. The evidence that the photocatalytic activity of these

materials may be related to both the distortion index of the octahedra and the DOS of the CB is in agreement with the literature [6–8].

5. Conclusion

Tantaloniobates with DJ perovskite structure were successfully synthesized by solid-state reaction. The $[MO_6]$ octahedron distortion index and the composition of the CB edge determined by theoretical calculations showed a great dependence on the type of element that occupies the *M* sites of the structure. Activity for hydroxyl radical photogeneration followed exactly the same increasing order of the octahedron distortion index, which is $KCa_2Ta_2NbO_{10} < KCa_2Ta_3O_{10} < KCa_2Nb_3O_{10} < KCa_2TaNb_2O_{10}$.

Declaration of Competing Interest

None.

Acknowledgments

This work was conducted during a visiting scholar period at Université de Rennes 1, sponsored by the Capes Foundation within the Ministry of Education, Brazil (grant n. BEX 88881.132329/2016-01). The computational facilities were supported by resources supplied by Brazilian Funding Agencies FAPESP, CNPq and the Center for Scientific Computing of the São Paulo State University (Grid Unesp). SEM experiments were performed on CMEBA platform (ScanMAT unit, UMS 2001, University of Rennes 1-CNRS).

Appendix A. Supplementary data

Supplementary data to this article can be found online at <https://doi.org/10.1016/j.matlet.2019.07.006>.

References

- [1] X. Zong, L. Wang, Ion-exchangeable semiconductor materials for visible light-induced photocatalysis, *J. Photochem. Photobiol. C* 18 (2014) 32–49, <https://doi.org/10.1016/j.jphotochemrev.2013.10.001>.
- [2] M.J. Geselbracht, H.K. White, J.M. Blaine, M.J. Diaz, J.L. Hubbs, N. Adelstein, J.A. Kurzman, New solid acids in the triple-layer Dion-Jacobson layered perovskite family, *Mater. Res. Bull.* 46 (2011) 398–406, <https://doi.org/10.1016/j.materresbull.2010.12.007>.
- [3] D. Jiang, T. Wang, Q. Xu, D. Li, S. Meng, M. Chen, Perovskite oxide ultrathin nanosheets/g-C₃N₄ 2D–2D heterojunction photocatalysts with significantly enhanced photocatalytic activity towards the photodegradation of tetracycline, *Appl. Catal. B* 201 (2017) 617–628, <https://doi.org/10.1016/j.apcatb.2016.09.001>.
- [4] D. Jiang, W. Ma, Y. Yao, P. Xiao, B. Wen, D. Li, M. Chen, Dion-Jacobson-type perovskite $KCa_2Ta_3O_{10}$ nanosheets hybridized with g-C₃N₄ nanosheets for photocatalytic H₂ production, *Catal. Sci. Technol.* 8 (2018) 3767–3773, <https://doi.org/10.1039/C8CY00930A>.
- [5] M.A. Bizeto, A.L. Shiguihara, V.R.L. Constantino, Layered niobate nanosheets: building blocks for advanced materials assembly, *J. Mater. Chem.* 19 (2009) 2512–2525, <https://doi.org/10.1039/B821435B>.
- [6] J. Sato, H. Kobayashi, Y. Inoue, Photocatalytic activity for water decomposition of indates with octahedrally coordinated d¹⁰ configuration. II. Roles of geometric and electronic structures, *J. Phys. Chem. B* 107 (2003) 7970–7975, <https://doi.org/10.1021/jp030021q>.
- [7] K. Maeda, Photocatalytic water splitting using semiconductor particles: History and recent developments, *J. Photochem. Photobiol. C* 12 (2011) 237–268, <https://doi.org/10.1016/j.jphotochemrev.2011.07.001>.
- [8] A. Kudo, Y. Miseki, Heterogeneous photocatalyst materials for water splitting, *Chem. Soc. Rev.* 38 (2009) 253–278, <https://doi.org/10.1039/b800489g>.
- [9] Y. Jing, B.P. Chaplin, Mechanistic study of the validity of using hydroxyl radical probes to characterize electrochemical advanced oxidation processes, *Environ. Sci. Technol.* 51 (2017) 2355–2365, <https://doi.org/10.1021/acs.est.6b05513>.
- [10] A.R.F.A. Teixeira, A.M. Neris, E. Longo, J.R.C. Filho, A. Hakki, D. Macphee, I.M.G. Santos, SrSnO₃ perovskite obtained by the modified Pechini method—Insights about its photocatalytic activity, *J. Photochem. Photobiol. A* 369 (2019) 181–188, <https://doi.org/10.1016/j.jphotochem.2018.10.028>.
- [11] R. Dovesi, A. Erba, R. Orlando, C.M. Zicovich-Wilson, B. Civalleri, L. Maschio, M. Rérat, S. Casassa, J. Baima, S. Salustro, B. Kirtman, Quantum-mechanical condensed matter simulations with CRYSTAL, *WIREs Comput. Mol. Sci.* 8 (2018), <https://doi.org/10.1002/wcms.1360>, e1360.
- [12] W.H. Baur, The geometry of polyhedral distortions. Predictive relationships for the phosphate group, *Acta Crystallogr. B* 30 (1974) 1195–1215, <https://doi.org/10.1107/S0567740874004560>.
- [13] A.S. Maia, F. Cheviré, V. Demange, V. Bouquet, M. Pasturel, S. Députier, R. Lebullenger, M. Guilloux-Viry, F. Tessier, Preparation of niobium based oxynitride nanosheets by exfoliation of Ruddlesden-Popper phase precursor, *Solid State Sci.* 54 (2016) 17–21, <https://doi.org/10.1016/j.solidstatesciences.2015.11.013>.
- [14] S.-H. Byeon, H.-J. Nam, Neutron Diffraction and FT-Raman Study of Ion-Exchangeable Layered Titanates and Niobates, *Chemistry of Materials* 12 (6) (2000) 1771–1778.
- [15] V. Džimbeg-Malčić, Ž. Barbarić-Mikočević, K. Itrić, Kubelka-Munk theory in describing optical properties of paper (I), *Tehnički Vjesnik* 18 (2011) 117–124, <https://hrcak.srce.hr/65936>.
- [16] M. Burbano, D.O. Scanlon, G.W. Watson, Sources of conductivity and doping limits in CdO from hybrid density functional theory, *J. Am. Chem. Soc.* 33 (2011) 15065–15072, <https://doi.org/10.1021/ja204639y>.